

Linear response of light deformed nuclei investigated by self-consistent quasiparticle random-phase approximation

C. Losa,¹ A. Pastore,² T. Døssing,¹ E. Vigezzi,⁴ and R. A. Broglia^{1,3,4}¹*The Niels Bohr Institute, University of Copenhagen, Blegdamsvej 17, 2100 Copenhagen Ø, Denmark*²*Department of Physics, Post Office Box 35 (YFL), FI-40014 University of Jyväskylä, Finland*³*Dipartimento di Fisica, Università degli Studi di Milano, via Celoria 16, I-20133 Milano, Italy*⁴*INFN, Sezione di Milano, via Celoria 16, I-20133 Milano, Italy*

(Received 23 February 2010; published 8 June 2010)

We present a calculation of the properties of vibrational states in deformed, axially-symmetric even-even nuclei, within the framework of a fully self-consistent quasiparticle random phase approximation (QRPA). The same Skyrme energy density and density-dependent pairing functionals are used to calculate the mean field and the residual interaction in the particle-hole and particle-particle channels. We have tested our software in the case of spherical nuclei against fully self-consistent calculations published in the literature, finding excellent agreement. We investigate the consequences of neglecting the spin-orbit and Coulomb residual interactions in QRPA. Furthermore we discuss the improvement obtained in the QRPA result associated with the removal of spurious modes. Isoscalar and isovector responses in the deformed $^{24-26}\text{Mg}$, ^{34}Mg isotopes are presented and compared to experimental findings.

DOI: [10.1103/PhysRevC.81.064307](https://doi.org/10.1103/PhysRevC.81.064307)

PACS number(s): 21.60.Jz, 21.30.Fe, 27.30.+t

I. INTRODUCTION

The response of many-body systems to an external, weakly coupled field provides much insight regarding the correlations existing among the particles composing the system, and the forces acting among them.

While the most familiar application of mean field theory is to describe stationary states, its extension to time-dependent states provides the basis for a theory of small amplitude oscillations known as random phase approximation (RPA) for normal systems and QRPA for superfluid (superconducting) systems displaying quasiparticle excitations.

Especially, small amplitude oscillations describe the dynamics of the nuclear surface. Couplings to the surface will influence the quasiparticle motion, renormalizing the effective mass (ω mass m_ω), in turn leading to couplings among the different vibrational modes.

A textbook example of such couplings is provided by the breaking of the giant dipole resonance in deformed nuclei (inhomogeneous damping [1–3]), in keeping with the fact that a permanent deformation can be viewed as a quadrupole vibration of finite inertia and of vanishing restoring force. Within this context we refer to Fig. 10 of Ref. [4], in particular to the two-peak photoabsorption cross section [$\sigma(E; E1)$] of the ^{150}Nd nucleus, marking the onset of static deformation in the neodymium isotopes as a function of mass number.

As the smooth increase of the FWHM of $\sigma(E; E1)$ as a function of A indicates, this cannot be a yes-or-no effect. In fact, the FWHM of $\sigma(E; E1)$ associated with the transitional nucleus ^{148}Nd is not very different from that of ^{150}Nd . Within this scenario, quadrupole deformations, static or dynamic, will also modify not only the properties (centroid and width) of the GDR but also those of the GQR and, in deformed nuclei, that of the GMR. The same line of reasoning also applies to other multipolarities of the static and dynamic deformations of the mean field, which should not necessarily be only quadrupolar.

Because exotic nuclei, in particular neutron halo nuclei are, as a rule, more polarizable than nuclei lying along the stability valley, one expects this to affect the modes and the associated renormalization to be especially important for such nuclei. Here, one may mention the pygmy resonance [5] and the inversion of the usual sequence of single particle energies [6]. A consistent treatment of the vibrational modes is the first step on the way to address such properties.

The low-frequency collective excitations are quite sensitive to the shell structure near the Fermi level as well as to the nuclear surface shape, and one expects that new kinds of collective excitation will emerge under new situations of nuclear structure. To investigate such possibilities, many calculations have been made using the self-consistent RPA based on the Skyrme-Hartree-Fock (SHF) method [7,8] and the quasiparticle-RPA (QRPA) including pairing correlations [9–14]. A number of similar approaches using different mean fields have also been carried out [15–22].

Recently new iterative methods have been developed to calculate RPA strength functions for both spherical [23] and deformed [24,25] nuclear systems. Low-frequency RPA modes in deformed nuclei close to the neutron drip line have been studied [26,27], taking also into account pairing correlations [28,29]. These latter calculations are based on a BCS approximation which does not take into account continuum coupling effects, typical of drip-line nuclei. A proper theoretical description of such weakly bound systems requires a careful treatment of the asymptotic part of the nucleonic density. An appropriate framework for these calculations is provided by the Hartree-Fock-Bogoliubov (HFB) formalism, solved in coordinate representation [30,31] especially for spherical nuclei [32], or more conveniently in the configuration-space approach for deformed nuclei [33].

A quantitative description of excitations in exotic nuclei is given by fully consistent QRPA calculations on top of an

HFB ground state, such that the same effective interaction is used for both calculations. A fully consistent HFB+QRPA approach with the Gogny effective interaction for spherical and deformed nuclei has been developed in a harmonic oscillator basis [34]. Standard QRPA equations have also been solved in a cylindrical box with the Skyrme effective interaction, not including neither spin-orbit effects nor the Coulomb residual interactions [35,36].

Within this context we discuss in the present paper a consistent approach to describe linear response in deformed nuclei within the framework of HFB+QRPA. Section II discusses the elements used to work out a software to implement such a program. In Sec. III, we provide detailed information regarding Hartree-Fock-Bogoliubov ground states. Section III also illustrates some basic results of the QRPA software developed by us to treat deformed nuclei when applied, for a consistency check, to the case of a spherical system. In this section we also carry out a discussion concerning the spurious modes. In Sec. IV the response functions of ^{20}O , $^{24-26}\text{Mg}$, and ^{34}Mg are shown and discussed in comparison to available data and to other calculations. Conclusions are drawn in Sec. V.

II. METHOD

As the first step in the self-consistent calculation of excitations in axially deformed and reflection symmetric nuclei, HFB equations are solved in a finite harmonic oscillator (HO) as well as in a transformed harmonic oscillator (THO) basis. In both cases, a discretization of the positive energy continuum is carried out. We use the new version [known as (101)] of the program HFBTHO [33], choosing for ^{20}O , $^{24-26}\text{Mg}$, and ^{34}Mg , a quasiparticle energy cutoff $E_{cut} = 50$ MeV, and set $N_{sh} = 15$ HO (THO) shells. This code allows to perform HFB calculations with arbitrary Skyrme functionals together with a density-dependent pairing δ interaction [37]

$$V_{\text{pair}}(\mathbf{r}, \mathbf{r}') = \frac{1 - P_\sigma}{2} \left[V_0 + \frac{V_1}{6} \rho_{00}^\gamma(\mathbf{r}) \right] \delta(\mathbf{r} - \mathbf{r}'), \quad (1)$$

$\rho_{00}(\mathbf{r})$ being the associated isoscalar density and P_σ the spin exchange operator. In the following, we use the Skyrme functional SkM* [38] and a pairing interaction with the same parametrization as that adopted in Ref. [35], i.e., for ^{20}O and $^{24-26}\text{Mg}$ we adopt the parameters $V_0 = -280$ MeV fm³, $V_1 = -18.75V_0$, $\gamma = 1$ while for ^{34}Mg $V_0 = -295$ MeV fm³, $V_1 = -18.75V_0$, $\gamma = 1$ are employed. It corresponds to a mixed surface-volume type of pairing potential.

We diagonalize the HFB Hamiltonian in configuration space. We then diagonalize the density matrix ρ obtaining the canonical basis. We have checked the numerical accuracy of the procedure comparing the quasiparticle energies obtained in the original diagonalization with those obtained diagonalizing the HFB Hamiltonian in the canonical basis. We have found that the values agree within 10^{-4} MeV. Finally, we switch to coordinate space, tabulating the canonical wave-functions together with their first and second derivatives in a grid of 30×30 (Gauss-Hermite) \times (Gauss-Laguerre) points for Gauss quadrature integration in cylindrical coordinates (r_\perp, z) .

The QRPA basis is obtained using pairs of these canonical wave functions such that the dimension of the QRPA-Hamiltonian matrix does not exceed the size 20000×20000 . For this purpose, one first omits the canonical states i that have single-particle energies ε_i greater than some $\varepsilon_{\text{crit}}$. A second cut is made excluding those QRPA quasiparticle pairs displaying occupation probabilities less than some small v_{crit}^2 or larger than $1 - v_{\text{crit}}^2$. In the following calculations these parameters are given the values $\varepsilon_{\text{crit}} = 200$ MeV and $v_{\text{crit}} = 10^{-2}$. The QRPA excited states $|\lambda\rangle$ are described in terms of the quasiboson operators

$$Q_\lambda^\dagger = \sum_{K < K'} (X_{KK'}^\lambda \alpha_K^\dagger \alpha_{K'}^\dagger - Y_{KK'}^\lambda \alpha_K \alpha_{K'}), \quad (2)$$

acting on the QRPA correlated vacuum $|\tilde{0}\rangle$ ($Q_\lambda |\tilde{0}\rangle = 0$).

The operators α_K^\dagger , α_K are the canonical quasiparticle creation and annihilation operators, respectively, and $X_{KK'}^\lambda$, $Y_{KK'}^\lambda$ are the amplitudes of the two quasiparticles excitations $\{K, K'\}$. The matrix elements between different QRPA basis states $\{K, K'\}$ and $\{L, L'\}$ are expanded respecting the selection rules of the vibration's quantum numbers Ω and π . That is $\Omega = \Omega_K + \Omega_{K'} = \Omega_L + \Omega_{L'}$ and $\pi = \pi_K \cdot \pi_{K'} = \pi_L \cdot \pi_{L'}$. Here, Ω is the projection of the angular momentum on the symmetry axis z and π is the parity. Details concerning the calculation of matrix elements are given in the Appendix.

III. BASIC RESULTS

A. HFB ground states

First, potential energy curves are calculated as a function of the deformation parameter β , defined as

$$\beta = \sqrt{\frac{\pi}{5}} \frac{\langle \hat{Q} \rangle_n + \langle \hat{Q} \rangle_p}{\langle r^2 \rangle_n + \langle r^2 \rangle_p}. \quad (3)$$

The quantity $\langle \hat{Q} \rangle_q$ is the average value of the quadrupole-moment operator $\hat{Q} = 2z^2 - r_\perp^2$ for protons ($q = p$) and neutrons ($q = n$). The QRPA calculation will be performed based on the HFB solution corresponding to the absolute minimum of the potential energy.

Figure 1 (left panel) shows the potential energy curves for the nucleus ^{24}Mg , comparing the results obtained in the HO and THO basis. One finds a pronounced minimum corresponding to the prolate deformation $\beta = 0.39$. Similar HFB calculations have been carried out for the other isotopes discussed in the following. The nucleus ^{20}O is found to be spherical, while ^{26}Mg is oblate ($\beta = -0.18$) and ^{34}Mg is prolate ($\beta = 0.36$). The ground state properties of the four mentioned nuclei in the HO and THO basis are summarized in Table I. We notice that the curves of Fig. 1 have a very similar behavior to that of Figs. 1 and 2 of Ref. [34]. Also for ^{26}Mg , the HFB potential as function of deformation exhibits the two minima given by S. Péru [34]. For ^{24}Mg , the energy curves displayed in Fig. 1 show a clear preference for the prolate shape, whereas for ^{26}Mg , the oblate minimum preferred by our calculations is only situated 0.3 MeV below a minimum at a prolate deformation. Actually, data as well as shell model calculations prefer the prolate shape [39,40].

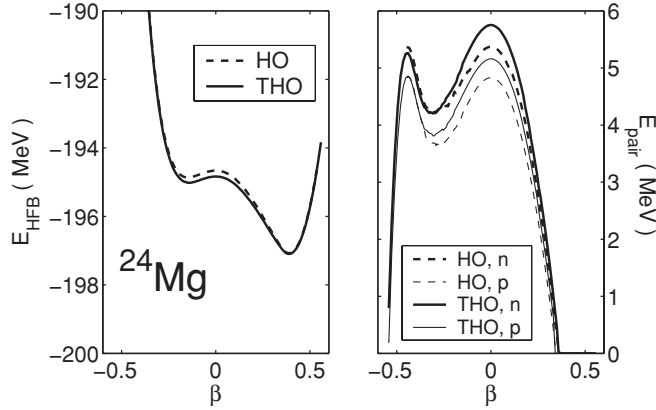


FIG. 1. HFB potential energy curves E_{HFB} (left hand panel); neutron (thick lines) and proton (thin lines) pairing energies E_{pair} (right hand panel). The quantities are calculated in HO (dashed curves) and THO (solid curves) basis as functions of axial deformation parameter β in the nucleus ^{24}Mg .

The right hand panel of Fig. 1 shows for ^{24}Mg the pairing energy $E_{\text{pair}} = \frac{1}{2}\text{Tr}(\Delta\kappa)$ calculated separately for protons and neutrons, where κ is the expectation value ($\langle\text{HFB}|P^+|\text{HFB}\rangle = \langle\text{HFB}|P|\text{HFB}\rangle$) in the superfluid ground state ($|\text{HFB}\rangle$) of the pair addition/removal ($P^+ = \sum_{\nu} c_{\nu}^{\dagger} c_{\bar{\nu}}^{\dagger} / P = \sum_{\nu} c_{\bar{\nu}} c_{\nu}$, c_{ν}^{\dagger} : single-particle creation operator) operator, that is of the pair field (abnormal density). Δ stands for the functional derivative of the energy $E[\rho, \kappa]$ with respect to the abnormal density (pairing gap) [33,41].

Returning now to Fig. 1 one may notice the difference between the curves for protons and neutrons. The Coulomb field influences the density of the nucleus and so the pairing interaction. At $\beta = 0.39$ the total pairing energy is zero, so QRPA calculations reduce to RPA ones where the excitations are only in the particle-hole (ph) channel. Full QRPA calculations are performed in the other three nuclear systems ^{20}O , ^{34}Mg , and ^{26}Mg for which the HFB ground state displays neutron and proton pairing correlations, respectively.

B. Response for the spherical nucleus ^{48}Ca

To test our deformed QRPA code developed on the basis of the deformed HFBTHO program by Stoitsov [33], we compare

TABLE I. Ground state properties of ^{20}O , $^{24,26,34}\text{Mg}$ obtained by the deformed HFB calculation in the HO and THO basis. Chemical potentials λ_q , deformations β_q , average pairing gaps Δ_q , root-mean-square radii $\sqrt{\langle r^2 \rangle_q}$ for neutrons ($q = n$) and protons ($q = p$), and the total binding energies E_{HFB} are listed.

	^{20}O HO	^{20}O THO	^{24}Mg HO	^{24}Mg THO	^{26}Mg HO	^{26}Mg THO	^{34}Mg HO	^{34}Mg THO
λ_n (MeV)	-7.18	-7.18	-14.13	-14.13	-13.12	-13.11	-4.17	-4.17
λ_p (MeV)	-17.27	-17.25	-9.51	-9.51	-11.05	-11.03	-20.19	-20.17
β_n	0.0	0.0	0.38	0.38	-0.16	-0.16	0.37	0.37
β_p	0.0	0.0	0.39	0.39	-0.16	-0.16	0.35	0.35
$\langle\Delta\rangle_n$ (MeV)	2.03	2.05	0.0	0.0	0.0	0.0	1.72	1.60
$\langle\Delta\rangle_p$ (MeV)	0.0	0.0	0.0	0.0	1.42	1.47	0.0	0.0
$\sqrt{\langle r^2 \rangle_n}$ (fm)	2.91	2.91	2.99	3.00	3.01	3.01	3.50	3.51
$\sqrt{\langle r^2 \rangle_p}$ (fm)	2.69	2.69	3.03	3.03	2.96	2.96	3.15	3.15
E_{HFB} (MeV)	-157.1	-157.2	-197.0	-197.0	-218.2	-218.3	-263.9	-263.9

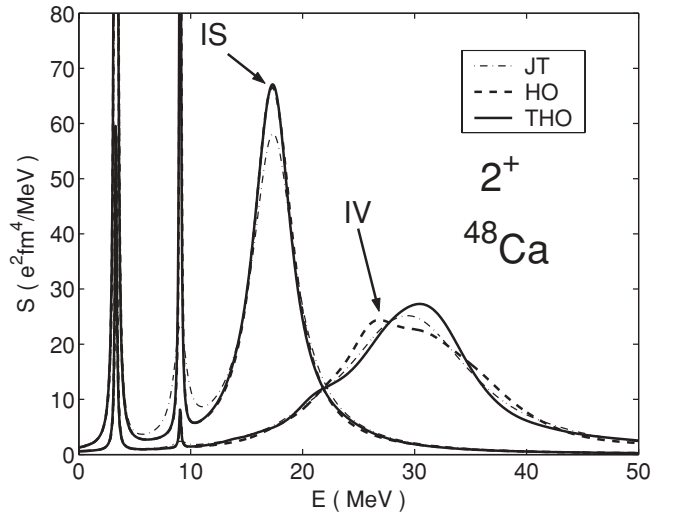


FIG. 2. Isoscalar (IS) and isovector (IV) 2^+ strength functions in ^{48}Ca in the spherical basis of J. Terasaki (JT, dashed-dotted curve), in the HO (dashed curve) and THO (solid curve) basis.

our results to those obtained with the spherical QRPA code developed by Terasaki *et al.* (JT) [14], making use of the same Skyrme interaction. Figure 2 shows, for the spherical nuclear system ^{48}Ca , such a comparison with calculations based on either (i) spherical basis states with a hard-wall boundary condition at 20 fm, and (ii) the two types of deformed basis, HO and THO. The response functions of Fig. 2 have been calculated with the help of Eqs. (1), (2) of Ref. [42]. In the following, we use strength functions defined as

$$S_J^\tau(E) = \sum_{\lambda} \sum_{\Omega} \frac{\Gamma/2}{\pi} \frac{|\langle\lambda|\hat{F}_{J\Omega}^\tau|0\rangle|^2}{(E - E_\lambda)^2 + \Gamma^2/4}, \quad (4)$$

for the multipole operator $\hat{F}_{J\Omega}^\tau$. If not specified in the text, the value $\Gamma = 1$ MeV is used as in Ref. [35] in the calculation of the IS monopole and quadrupole transition operators

$$\hat{F}_{2\Omega}^{IS} = \frac{eZ}{A} \sum_{i=1}^A r_i^2 Y_{2\Omega}(r_i), \quad (5)$$

$$\hat{F}_{00}^{IS} = \frac{eZ}{A} \sum_{i=1}^A r_i^2, \quad (6)$$

and for the IV dipole operator

$$\hat{F}_{1\Omega}^{IV} = \frac{eN}{A} \sum_{i=1}^Z r_i Y_{1\Omega}(\hat{r}_i) - \frac{eZ}{A} \sum_{i=1}^N r_i Y_{1\Omega}(\hat{r}_i). \quad (7)$$

The agreement between the strength functions labeled JT [42] with those labeled HO and THO shown on Fig. 2 is actually quite rewarding, in keeping with the completely different routes taken in the calculations. In all the three cases the strength function exhausts about 98% of the energy weighted sum rule (EWSR).

For the 2^+ mode in ^{48}Ca , the degeneracy between the components $\Omega^\pi = 0^+, \pm 1^+, \pm 2^+$ is reached up to the order of 10^{-3} in both the HO and THO basis.

C. Self-consistency and spurious states

Let us now turn to the spurious solutions of the QRPA equations in the dipole modes with $\Omega^\pi = 0^-, \pm 1^-$ and in the quadrupole modes with $\Omega^\pi = \pm 1^+$. Spurious modes are, in the present case, due to the translational and rotational symmetry breaking, respectively, of the HFB ground state [41]. The quadrupole modes with $\Omega^\pi = 0^+$ also contains spurious states associated with particle-number nonconservation. Former works on QRPA both for spherical nuclei [14] and for deformed ones [34] show that the spurious states which should be at zero energy [43] have instead values from a few keV to 1–1.8 MeV, well separated from, in any case, (physical) states. These nonzero energies may be taken as a measure of numerical accuracy with which linear response is calculated, and are strongly related to the choice of basis states and truncation of basis size.

The spurious states obtained in our fully consistent calculations lie either on the real on the imaginary axis, and their absolute value never exceeds 700 keV. In Figs. 3 and 4 we show results for ^{24}Mg , comparing the self-consistent results with those obtained (i) neglecting both Coulomb and spin-orbit residual interaction and (ii) neglecting only the Coulomb residual interaction. It is seen that the absolute values of the energies are progressively reduced going from case (i) (about 3 MeV) to case (ii) (2–2.2 MeV) and finally to the self-consistent solution (less than 0.5 MeV). One also notes that in case (i) the energies of the spurious states lie on the real axis, while in case (ii) they are found on the imaginary axis. The fully consistent QRPA calculations give imaginary energies for the dipole spurious modes and real energies for the quadrupole spurious modes, all below 500 keV. It is satisfactory that the energies of the spurious modes get closer to zero as more terms of the residual interaction are included. We ascribe the remaining distance to zero to the truncation of the basis and to numerical inaccuracies. Within this scenario one may posit that a spurious mode obtained by fully consistent QRPA calculations at “imaginary energy” 100–500 keV is as good a solution as that corresponding to a spurious real energy mode at 100–500 keV.

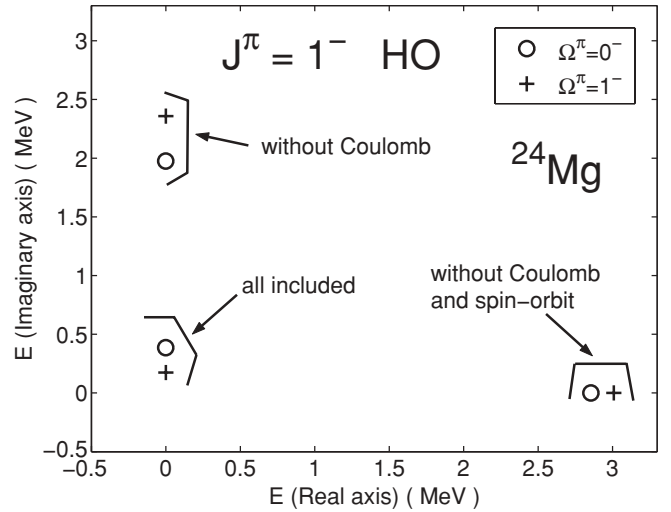


FIG. 3. Energies on the complex plane of the spurious state for the 1^- mode with $\Omega^\pi = 0^-$ (circles) and $\Omega^\pi = 1^-$ (crosses) projections in ^{24}Mg in HO basis. The figure illustrates the change in energy of spurious modes when specific terms of the interaction are omitted.

A similar study has been performed on the energies of the dipole spurious modes of ^{20}O . Also for this nucleus if both Coulomb and spin-orbit parts are neglected, the spurious energies are at 2.5–3 MeV. The values jump to about 1.5–2 MeV on the imaginary axis if one adds the spin-orbit contribution to the residual interaction. Finally, the energy of a spurious state obtained with a fully consistent QRPA calculation can be real or imaginary not exceeding 600 keV. For the deformed nuclei ^{26}Mg and ^{34}Mg we obtain from the fully consistent QRPA calculations with $\Omega^\pi = 0^-, \pm 1^-$ and $\Omega^\pi = \pm 1^+$ spurious states with either real or imaginary energy, in any case the modulus not exceeding 700 keV. For ^{20}O and $^{26,34}\text{Mg}$ the quadrupole spurious modes with $\Omega^\pi = 0^+$ are all real at around 1.8–2 MeV. We ascribe this problem concerning the $\Omega^\pi = 0^+$ modes mainly to the rather crude cut in the occupation probability given by $v_{\text{crit}} = 10^{-2}$. We have

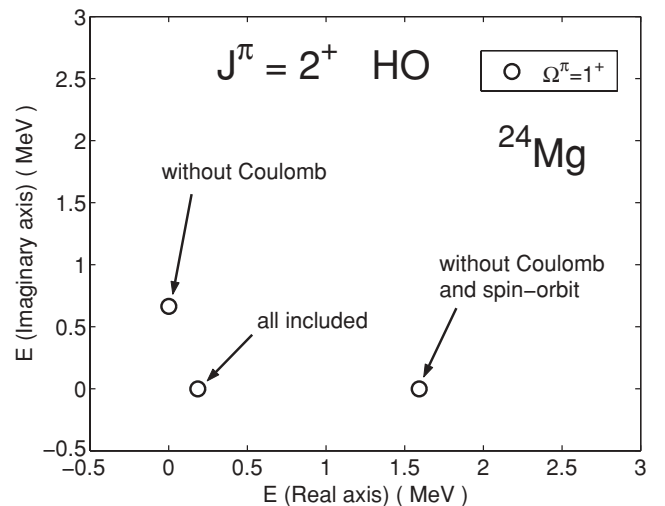


FIG. 4. The same as Fig. 3 but for the 2^+ mode with $\Omega^\pi = 1^+$ projection.

checked in the case of ^{26}Mg that reducing the value of v_{crit} to 10^{-3} brings the energy of the 0^+ spurious state from 1.8 MeV (on the real axis) down to 1.1 MeV (on the imaginary axis). The transition strength is only affected for energies below about 3 MeV.

Similar investigations of the spurious modes for calculations with the Gogny force have been reported by Peru *et al.* in Refs. [44] and [34] for spherical and deformed shapes, respectively. For spherical nuclei, it is found that the spurious modes lie at very low energy, about 3–5 keV, when all terms of the interaction are included, whereas they may move up to about 2 MeV when leaving out parts of the interaction. For deformed nuclei [34], the result is qualitatively the same as in the present work. However, the Gogny results are better for the $\Omega^\pi = 0^+$ mode, which comes at a very low energy, but worse for the translational invariance modes $\Omega^\pi = 0^-, \pm 1^-$, where the spurious mode energies can come as high as 1.8 MeV.

IV. STRENGTH FUNCTIONS

A. ^{20}O

The IS quadrupole 2^+ mode is shown in Fig. 5, calculated with the HO as well as with the THO basis states. A large fraction of the strength function is concentrated in three energy regions: a low-lying mode around 3 MeV, a small peak around 10 MeV, and a giant resonance around 20 MeV. The two calculations display a remarkable agreement with respect to the strength function below 15 MeV. Whereas the calculations agree on the centroid and the strength of the giant resonance, they display differences with respect to the splitting of the two components of the resonance, and on the distribution of strength between the two peaks. When we omit both the spin-orbit and Coulomb residual interaction, in the giant resonance region the strength functions are shifted down in energy about 0.3 MeV for both the basis used, and the peak

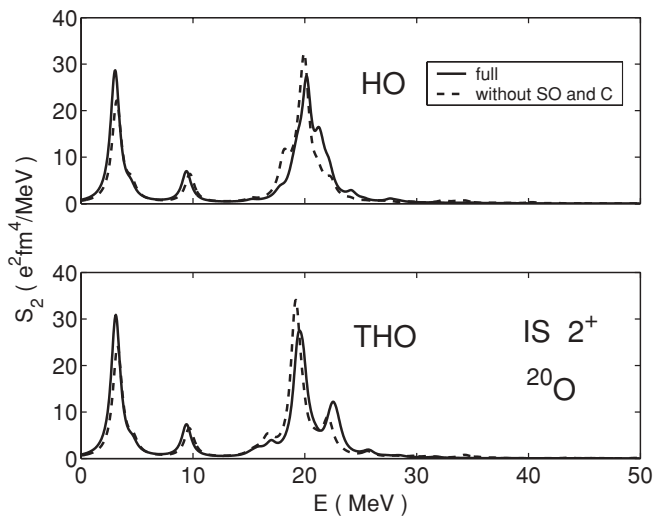


FIG. 5. IS 2^+ strength functions in ^{20}O , in HO (upper panel) and THO (lower panel) basis without the residual spin-orbit (SO) and Coulomb (C) interaction (dashed curve) and with all the terms included (solid curve).

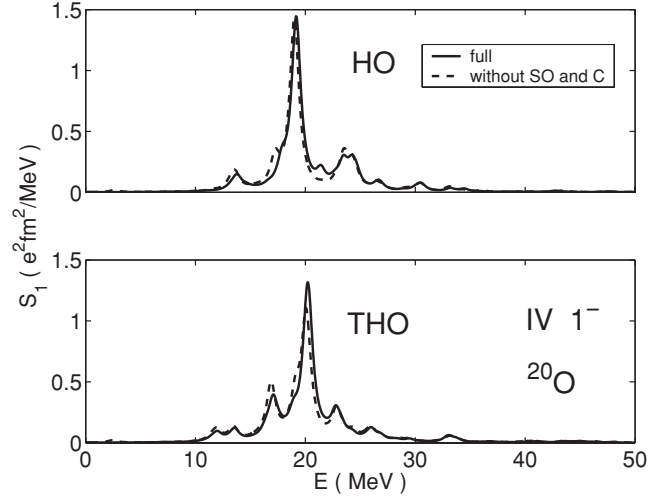


FIG. 6. The same as Fig. 5 but for IV 1^- strength functions.

heights increase by 15% for HO and 25% for THO. Concerning the two peak energies below 10 MeV, they are both shifted up by about 0.2 MeV while the peak heights are lowered by 20% for both the two basis.

Figure 6 shows the IV giant dipole resonance in the energy range (15–25) MeV. In the THO basis the peak is at 20.2 MeV, while that in the HO basis is shifted down about 1 MeV.

The strength functions calculated without the spin-orbit and Coulomb interactions can be compared to those obtained by Yoshida *et al.* [35], who did not include these terms. We find a very good overall agreement. On closer inspection, the energy of the giant resonance peaks in our calculation in the THO basis is about 0.3 MeV higher than in Ref. [35].

B. $^{24,26}\text{Mg}$

1. IS 2^+ modes

In Figs. 7 and 8 we display the response functions of the IS quadrupole mode of the deformed prolate and oblate $^{24,26}\text{Mg}$ isotopes.

For both these nuclei, the first low-lying state is found to have projection $\Omega = 2^+$, corresponding to a γ vibration, while the β vibration with $\Omega = 0^+$ is situated at a considerably higher energy. Comparing the nuclei, one sees that ^{24}Mg , which may be described as a deformed closed shell nucleus for the prolate shape, is more stiff toward vibrations than the oblate ^{26}Mg . This is all in qualitative accordance with data [45]. However, a more careful comparison of calculations and data reveal some discrepancies, especially for ^{26}Mg .

In ^{24}Mg , the calculated energy of the lowest $\Omega^\pi = 2^+$ is 4.14 MeV, to be compared to the experimental value 4.23 MeV of the γ -band head, the state 2_2^+ [45]. Likewise, the calculated energy of the lowest $\Omega^\pi = 0^+$ is 7.08 MeV, should be compared to the experimental value 6.43 MeV. Both these states are not very collective, composed equally of proton and neutron particle-hole excitations: $[N, n_z, \Lambda, \pm\Omega^\pi] \equiv [2, 1, 1, \pm\frac{3}{2}^+] \rightarrow [2, 1, 1, \pm\frac{1}{2}^+]$ for the $\Omega = 2^+$ state and $[2, 2, 0, \pm\frac{1}{2}^+] \rightarrow [2, 1, 1, \pm\frac{1}{2}^+]$ for the $\Omega = 0^+$ state,

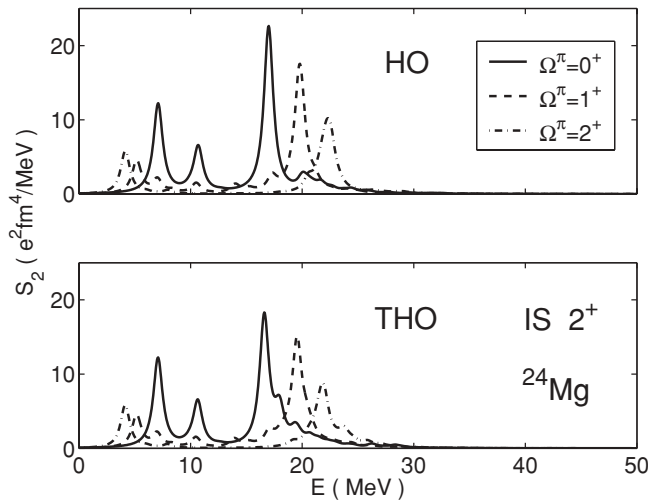


FIG. 7. IS 2^+ strength functions in ^{24}Mg , in HO (upper panel), and THO (lower panel) basis for the $\Omega^\pi = 0^+$ (solid curve), 1^+ (dashed curve), and 2^+ (dashed-dotted curve) excitations.

respectively. Still, the RPA root is shifted down in energy by about 1.5 MeV relative to the single ph excitations. These assignments are in reasonable accordance with experimental information from γ decay [45], particle transfer [46], (e, e') inelastic scattering [47], (α, α') scattering [48], and (π, π') scattering [49].

In ^{26}Mg , the lowest $\Omega^\pi = 2^+$ excitation is calculated to be at 1.31 MeV, considerably below the experimental state 2_2^+ at 3.0 MeV, while the lowest $\Omega^\pi = 0^+$ excitation is at 2.75 MeV, to be compared to the state 0_2^+ at 3.59 MeV. Compared to ^{24}Mg , the $\Omega^\pi = 2^+$ excitation is predicted to be more collective. This is not in accordance with the experimental $B(E2)$ values from the ground state, which are of about equal magnitude for the two nuclei. Also, the considerable matrix element for exciting the $\Omega^\pi = 0^+$ state predicted by the calculations is in

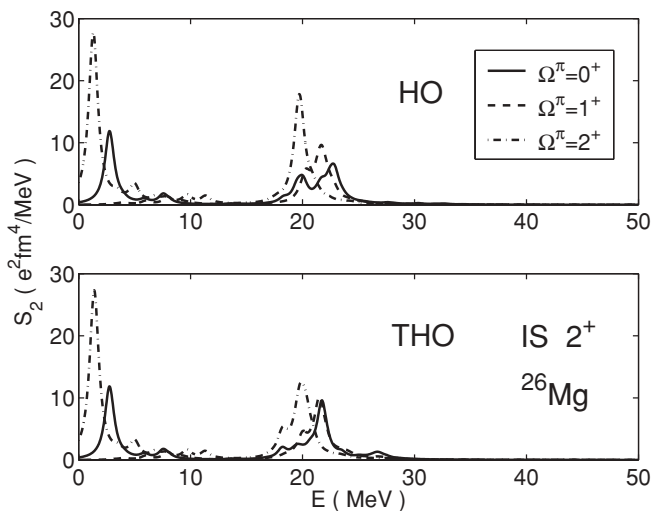


FIG. 8. IS 2^+ strength functions in ^{26}Mg , in HO (upper panel), and THO (lower panel) basis for the $\Omega^\pi = 0^+$ (solid curve), 1^+ (dashed curve), and 2^+ (dashed-dotted curve) excitations.

disagreement with the long lifetime seen experimentally of the 0_2^+ state. For ^{26}Mg , this comparison between data and our calculations of the low lying states may be rather uncertain due to the close competition between prolate and oblate states.

The rather low collectivity of the β - and γ -vibrations follows a general trend. With a permanent deformation, most of the quadrupole collectivity is tied up in the deformation of the mean field. This will in turn influence the renormalization effects these modes will have on the single particle motion. In this context, one can quote the rather different pattern observed in the distribution of matrix elements contributing to the induced pairing interaction in spherical and deformed nuclei, respectively [50,51].

Next, we turn our attention to the giant vibrations situated in the energy region 15–25 MeV for all cases, with a characteristic splitting between the different projections Ω . For the prolate nucleus ^{24}Mg , the $\Omega^\pi = 0^+$ vibration is along the longest axis and acquires the lowest energy. For the oblate nucleus ^{26}Mg , the opposite behavior is observed, and here the splitting is less pronounced due to the smaller value of the deformation parameter [3].

In Tables II and III the mean energies

$$E(GR) = \frac{m_1[E_{\min}, E_{\max}]}{m_0[E_{\min}, E_{\max}]}, \quad (8)$$

with moments

$$m_\lambda[E_{\min}, E_{\max}] = \sum_k \sum_\Omega E_k^\lambda |\langle k | \hat{F}_{J\Omega} | 0 \rangle|^2, \quad (9)$$

calculated for the 2^+ modes of $^{24,26}\text{Mg}$ in the energy range $[E_{\min}, E_{\max}] = [9, 41]$ MeV, are given in HO and THO basis. First, one sees that the mean value in the giant resonance region is practically not affected by the choice of basis. Secondly, one may address the 1 MeV difference between the results obtained with the SkM* Skyrme force and those with the Gogny force, by Péru *et al.* [34]. Part of this difference may be caused by the lower effective mass $m^*/m = 0.7$ for the Gogny force, as

TABLE II. Theoretical mean energy values (in MeV) obtained with the Gogny force by Péru *et al.*, with the SkM* and SLy4 Skyrme force in HO and THO basis (present work), and experimental mean energy values by Youngblood *et al.* and Irgashev *et al.* of the IS giant monopole, quadrupole resonances (calculated in the energy interval $[E_{\min}, E_{\max}] = [9, 41]$ MeV) and IV giant dipole resonances (calculated in the energy interval $[E_{\min}, E_{\max}] = [10, 29]$ MeV) in ^{24}Mg .

^{24}Mg	IS	IS	IV
$E(GR)$	$J^\pi = 0^+$	$J^\pi = 2^+$	$J^\pi = 1^-$
Interval	[9,41]	[9,41]	[10,29]
Theor. D1S (Péru <i>et al.</i>)	21.0	20.5	23.0
Theor. SkM* (HO)	20.7	19.4	19.6
Theor. SkM* (THO)	20.3	19.3	19.8
Theor. SLy4 (HO)		20.0	19.8
Theor. SLy4 (THO)		19.9	19.8
Exp. (Youngblood <i>et al.</i>)	21.0 ± 0.6	16.9 ± 0.6	
Exp. (Irgashev <i>et al.</i>)			22.1

TABLE III. Theoretical mean energy values (in MeV) obtained with the Gogny force by Péru *et al.*, with the SkM* Skyrme force in HO and THO basis (present work) of the IS giant monopole, quadrupole resonances (calculated in the energy interval $[E_{\min}, E_{\max}] = [9, 41]$ MeV), and of the IV giant dipole resonance (calculated in the energy interval $[E_{\min}, E_{\max}] = [10, 29]$ MeV) in ^{26}Mg . For this last resonance the experimental mean energy value by Fultz *et al.* is also given.

^{26}Mg	IS	IS	IV
$E(GR)$	$J^\pi = 0^+$	$J^\pi = 2^+$	$J^\pi = 1^-$
Interval	[9,41]	[9,41]	[10,29]
Theor. D1S (Péru <i>et al.</i>)	22.0	21.0	22.9
Theor. SkM* (HO)	22.1	20.3	20.3
Theor. SkM* (THO)	21.9	20.3	20.2
Exp. (Fultz <i>et al.</i>)			20.6

compared to $m^*/m = 0.8$ for the SkM* force. For this reason we performed for ^{24}Mg a calculation also with a SLy4 force where $m^*/m = 0.7$. The centroid energy then increases by roughly 0.6 MeV, indicating that about half of the difference between the two calculations can be ascribed to the effective mass. Finally, the results may be compared to the experimental mean energy of 16.9 ± 0.6 obtained by Youngblood *et al.* [52], and one sees that all the theoretical calculations overshoot this value by at least 2 MeV.

The theoretical results obtained in the present work with the SkM* and SLy4 forces exhaust 83–84 % of the EWSR exceeding the experimental result by about 20%. This difference in the EWSR as well as in the mean energy between the present work and the experimental data of Youngblood *et al.*, is apparent from Fig. 9, which shows the comparison between calculated and experimental strength functions. The

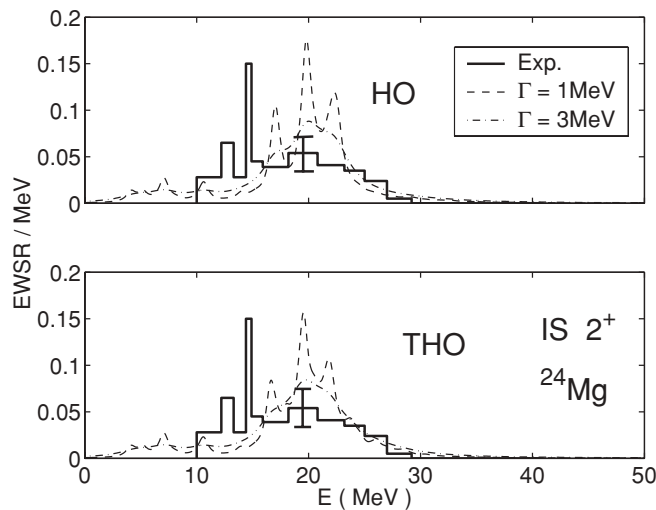


FIG. 9. Fractions of IS quadrupole EWSR in ^{24}Mg , in HO (upper panel) and THO (lower panel) basis. Dashed and dot-dashed curves are obtained from folding of QRPA spectra with a Lorentian distribution having $\Gamma = 1$ MeV and $\Gamma = 3$ MeV, respectively. These are compared with the experimental data by Youngblood *et al.* (solid curve).

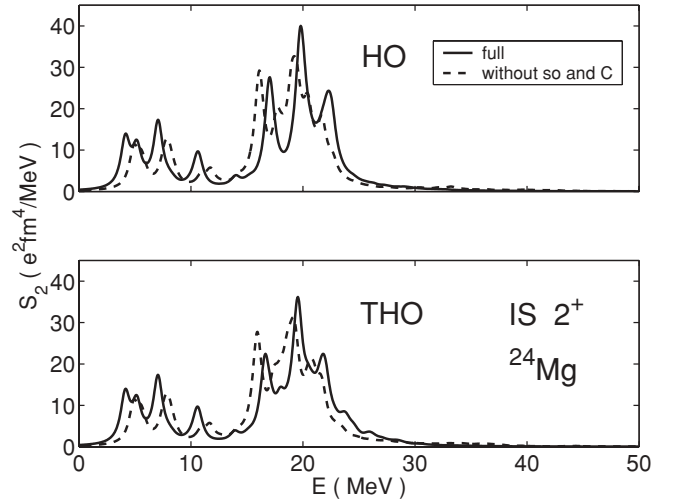


FIG. 10. IS 2^+ strength functions in ^{24}Mg , in HO (upper panel) and THO (lower panel) basis without the residual spin-orbit (SO) and Coulomb (C) interaction (dashed curve) and with all the terms included (solid curve).

shape of the experimental curve is reproduced in its overall features, in particular for $\Gamma = 3$ MeV. However, according to the calculations, the central peak around 20 MeV is too pronounced, and there is too little strength toward lower energies. It is of notice the sharp peak experimentally observed at 15 MeV. To which extent it may be connected with the $\Omega^\pi = 0^+$ mode which in our calculations appear blue shifted by 2.5 MeV (i.e., at 17.5 MeV) is an open question.

Figure 10 shows for ^{24}Mg the effect of leaving out the spin-orbit and Coulomb parts of the residual interaction. One sees that this would lead to a downward shift of the giant resonance by about 0.9 MeV. Comparing to the work of Yoshida *et al.* [35] one finds that their peaks are shifted further down by about 0.9 MeV with respect to those obtained in the present work without the spin-orbit and Coulomb terms. This remaining shift should be compared to the equivalent shift of 0.3 MeV discussed above for ^{20}O . It should be ascribed to the differences between the two calculations, the renormalization of the interaction in Ref. [35], and the different basis used.

2. IV 1^- modes

Figures 11 and 12 show the response functions of the IV dipole modes, of the deformed prolate and oblate $^{24,26}\text{Mg}$ isotopes. The IV giant dipole resonances show a two-peaked structure. For both nuclear systems the low-lying part of the resonances is given by a defined peak at around 16 MeV and 18 MeV for ^{24}Mg and ^{26}Mg , respectively. The higher energy part of the strength is fragmented, especially for the THO basis, in fair agreement with the responses given by Péru *et al.* [34]. In the HO approach one may see a two-peaked structure up to around 26 MeV for ^{24}Mg and a defined peak at 21–22 MeV for ^{26}Mg .

The fraction of the EWSR in ^{24}Mg for the IV 1^- mode calculated in the present work for two values of Γ is compared to the experimental ones [53] in Fig. 13. The theoretical and

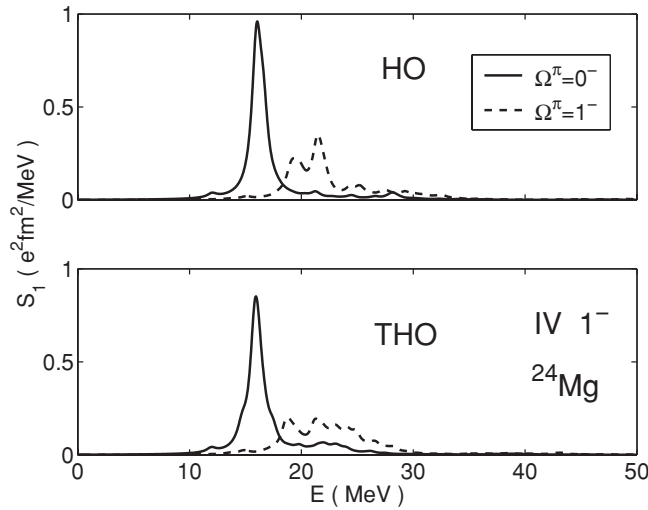


FIG. 11. IV 1^- strength functions in ^{24}Mg , in HO (upper panel), and in THO (lower panel) basis for the $\Omega^\pi = 0^-$ (solid curve), 1^- (dashed curve) excitations.

experimental curves show the same two-peak structure, but the calculated peaks appear at energies which are about 3 MeV too low. This difference with the experimental dipole response is also found in the calculations by Inakura *et al.* [25]. In fact, the experimental mean energy that we extract from the data in the range $[E_{\min}, E_{\max}] = [15, 30]$ MeV is equal to 22.1 MeV, to be compared with our value of 19.8 MeV. The Gogny-force calculation by Péru *et al.* [34] instead displays the peaks at about the observed energies, with a mean energy of 23.0 MeV (cf. Table II).

One may comment that the excitation energies of the lowest peak predicted by our calculation (17 MeV) is just above the threshold for particle emission. At these energies, a considerable part of photon absorption events will lead to a γ -ray cascade rather than particle emission. In fact, the $^{24}\text{Mg}(e, e')$ inelastic scattering experiment by Titze

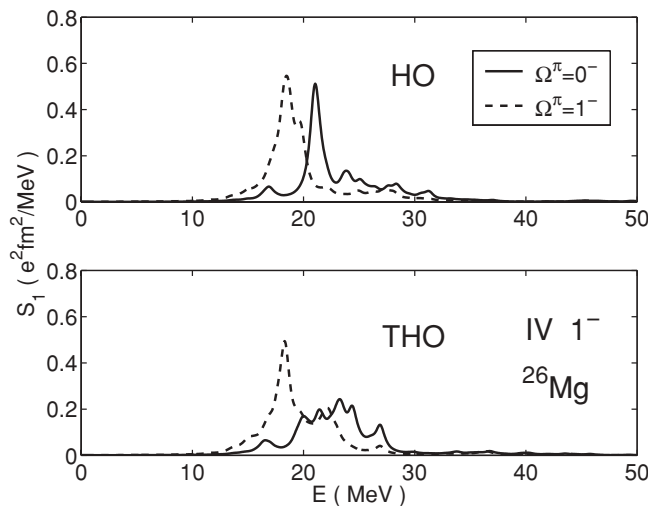


FIG. 12. IV 1^- strength functions in ^{26}Mg , in HO (upper panel), and in THO (lower panel) basis for the $\Omega^\pi = 0^-$ (solid curve), 1^- (dashed curve) excitations.

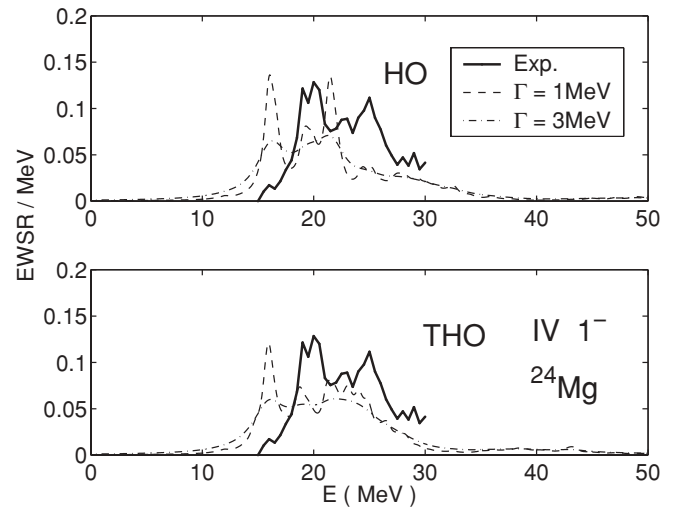


FIG. 13. Fractions of IV dipole EWSR in ^{24}Mg , in HO (upper panel), and in THO (lower panel) basis. Dashed and dot-dashed curves are obtained from folding of QRPA spectra with a Lorentian distribution having $\Gamma = 1$ MeV and $\Gamma = 3$ MeV, respectively. These are compared with the experimental data by Irgashev *et al.* (solid curve).

et al. [54] displays a peak around 17 MeV (split into two rather narrow components), whereas the (γ, n) and (γ, p) data only display a tiny and statistically insignificant peak at this energy. On the other hand, (e, e') reactions are more complicated to analyze theoretically in a precise way than hadronic inelastic processes and photon absorption, since a consistent calculation of the cross section should go beyond the long wavelength approximation, and also take into account magnetic interactions.

For ^{26}Mg , the fractions of the EWSR may be compared to three experiments [55–57]. Figure 14 displays the comparison

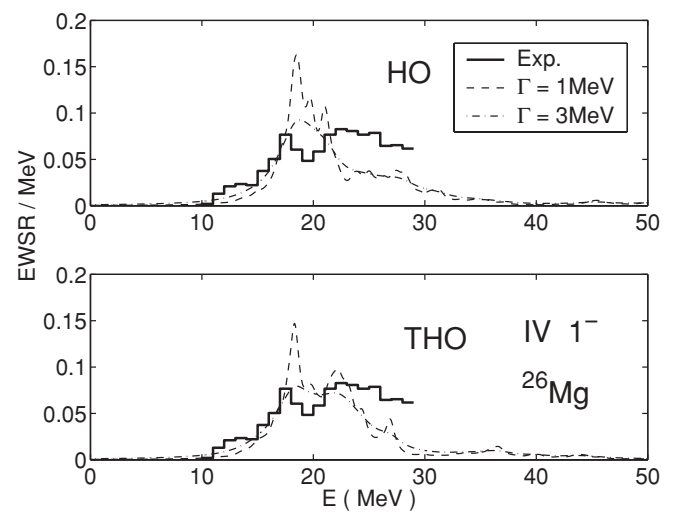
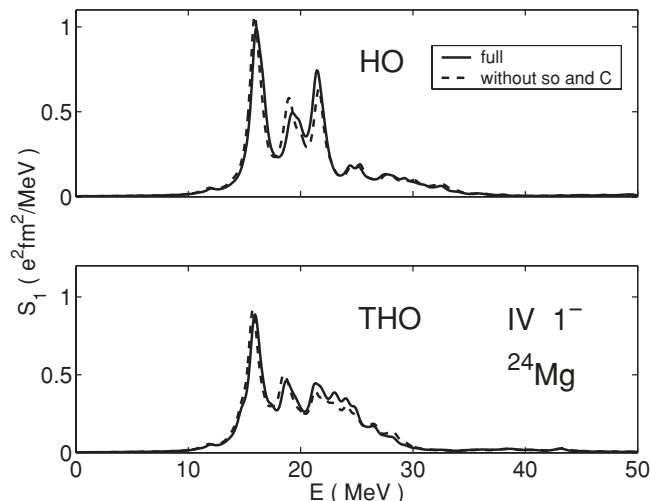


FIG. 14. Fractions of IV dipole EWSR in ^{26}Mg , in HO (upper panel), and in THO (lower panel) basis. Dashed and dot-dashed curves are obtained from folding of QRPA spectra with a Lorentian distribution having $\Gamma = 1$ MeV and $\Gamma = 3$ MeV, respectively. These are compared with the experimental data by Fultz *et al.* (solid curve).


 FIG. 15. The same as Fig. 10 but for IV 1^- strength functions.

between our curves and that of Fultz *et al.* [56] who, with respect to the more recent work of Ishkhanov *et al.* [57], also measure the $^{26}\text{Mg}(\gamma, pn)$ cross section. The three experiments agree with each other with respect to the overall width of the $E1$ response, and they all display two maxima at 18 MeV and 22 MeV separated by a shallow minimum around 20 MeV. This is in qualitative agreement with our calculated curves, especially when the THO basis is used and the QRPA spectra is folded with a Lorentian distribution with $\Gamma = 3$ MeV.

Combining the information from Tables II and III, one notices that calculations based on a given interaction predict a rather small shift of the mean energy of the giant dipole resonance, when comparing the two nuclei, ^{24}Mg and ^{26}Mg . This is at variance with experiment, according to which the mean energy shifts down by 1.7 MeV. In this way, a calculation which is in accordance with the data for ^{24}Mg , will disagree with data for ^{26}Mg , and viceversa.

For completeness Fig. 15 shows the effect of leaving out the spin-orbit and Coulomb part of the interaction and one sees that this has only a minor effect contrary to the considerable effect obtained for the quadrupole mode.

3. IS 0^+ modes

In Fig. 16 we display the experimental fraction of EWSR of Youngblood *et al.* [52] and those obtained in the present work for the IS monopole mode of ^{24}Mg . The theoretical response shows a two-peak structure, with a low energy peak well defined around 18 MeV and a fragmented high energy component which appears to be more sensitive to details and to the choice of the basis. Indeed, in the HO basis there is a significant contribution around 22 MeV, while in the THO basis this is in the energy range 25–30 MeV. Such peaks are not observed in the experimental curve, which is quite flat and covers a broad energy interval. Except for the peaks, this spread-out behavior of the strength function is also found in the calculations. Also for the monopole mode, the calculated EWSR of 90% is larger than the experimental value, $72 \pm 10\%$. From the similarity of the shape of the curves one can

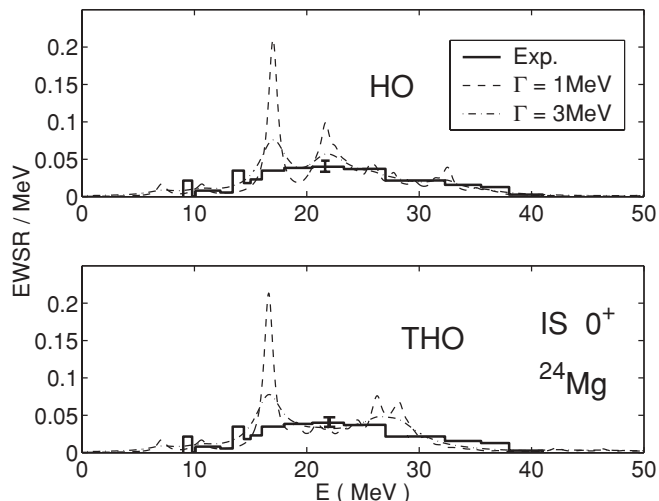


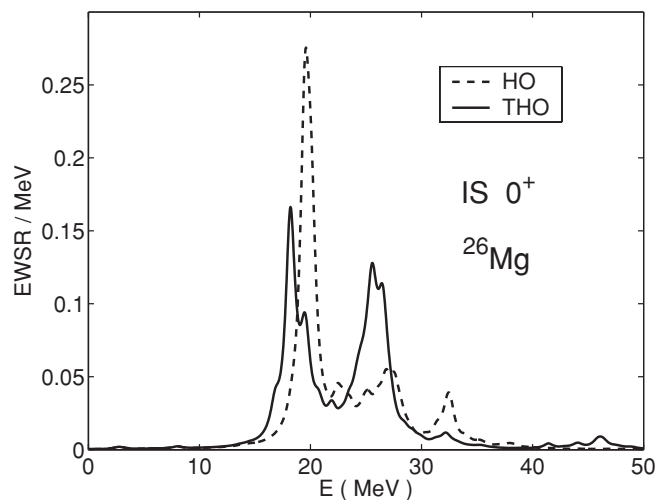
FIG. 16. The same as Fig. 9 but for fractions of IS monopole EWSR.

expect that the calculated centroids and the experimental ones are in good agreement, as given by the numbers of Table II.

Figure 17 shows the calculated fraction of EWSR for the IS monopole mode of ^{26}Mg . As for ^{24}Mg , the behavior of the response is quite sensitive to the choice of the basis. The curve displayed in the HO basis has a behavior similar to that obtained by Péru *et al.* [34], i.e., the resonance has a prominent peak around 20 MeV and a broad component at higher energy. In the THO basis the low-energy peak of the resonance is shifted down by 1.5 MeV and there is a significant contribution around 26 MeV.

C. ^{34}Mg

Figure 18 shows the calculated IS quadrupole strength functions for the neutron-rich nucleus ^{34}Mg in the HO and THO basis. One can see a low-lying peak at 2–3 MeV


 FIG. 17. Fractions of IS monopole EWSR in ^{26}Mg , in HO basis (dashed curve) and THO (solid curve) basis.

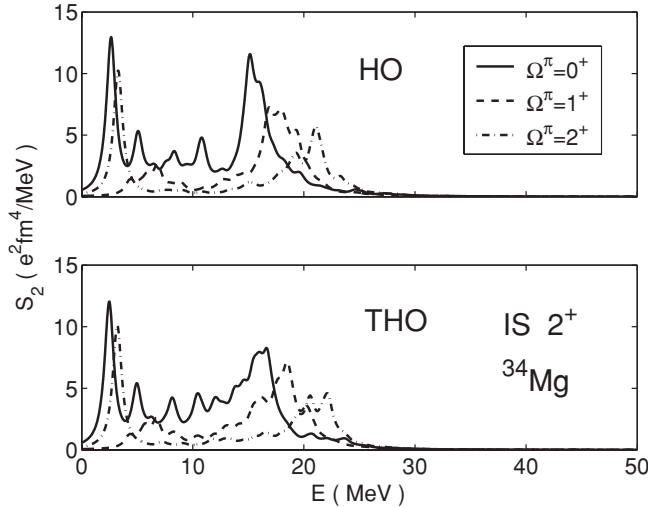


FIG. 18. IS 2^+ strength functions in ^{34}Mg , in the HO (upper panel) and in the THO (lower panel) basis for the $\Omega^\pi = 0^+$ (solid curve), 1^+ (dashed curve), and 2^+ (dashed-dotted curve) excitations.

and a giant resonance at 15–22 MeV. The first low-lying state belongs to the $\Omega^\pi = 0^+$ component and it is mainly constructed by the neutron pp excitations $[N, n_z, \Lambda, \pm\Omega^\pi] \equiv [2, 0, 2, \pm\frac{3}{2}^+]^2, [3, 2, 1, \pm\frac{3}{2}^+]^2, [3, 3, 0, \pm\frac{1}{2}^-]^2$, the first of them coming from $(1d_{3/2})^2$ the latter two from $(1f_{7/2})^2$. The features of these transitions are shown in Tables IV and V for the HO and THO basis, respectively. These results are in fair agreement with those of Table I of Ref. [36]. One may notice that the two approaches give basically the same results and that the difference of about 200 keV between the two energy peaks (2.64 MeV in the HO basis and at 2.48 MeV in the THO basis) is due to the unperturbed 2qp transitions with energy $E_{qpK} + E_{qpK}$. The quasiparticle energies E_{qpK} are obtained diagonalizing the HFB Hamiltonian in the canonical basis (we refer to Eqs. (4.14b), (4.20) of Ref. [58]). From the values of these 2qp energy transitions one may conclude that the main contribution of the residual interaction is to shift down in energy the IS quadrupole response, rather independently on the choice of basis.

TABLE IV. QRPA amplitudes $[N, n_z, \Lambda, \pm\Omega^\pi]_K^2$ with isospin q ($q = n$ for neutrons, $q = p$ for protons) of the IS quadrupole $\Omega^\pi = 0^+$ mode at 2.64 MeV for the HO basis in ^{34}Mg . The quasiparticle occupations v_K^2 , the single particle energies ε_K , and the 2qp excitation energies $E_{qpK} + E_{qpK}$, are given. Only components with $X_{KK}^2 - Y_{KK}^2 > 0.01$ are listed.

KK	$[2, 0, 2, \pm\frac{3}{2}^+]^2$	$[3, 2, 1, \pm\frac{3}{2}^-]^2$	$[3, 3, 0, \pm\frac{1}{2}^-]^2$
q_K	n	n	n
v_K^2	0.25	0.68	0.92
ε_K	-3.18	-4.91	-6.84
X_{KK}	-0.64	0.65	0.29
Y_{KK}	-0.08	0.03	0.04
$E_{qpK} + E_{qpK}$	3.79	3.72	5.96

TABLE V. The same as Table IV but for the THO basis at 2.48 MeV.

KK	$[2, 0, 2, \pm\frac{3}{2}^+]^2$	$[3, 2, 1, \pm\frac{3}{2}^-]^2$	$[3, 3, 0, \pm\frac{1}{2}^-]^2$
q_K	n	n	n
v_K^2	0.24	0.70	0.92
ε_K	-3.20	-4.91	-6.84
X_{KK}	-0.64	0.67	0.27
Y_{KK}	-0.09	0.03	0.04
$E_{qpK} + E_{qpK}$	3.58	3.49	5.72

In Fig. 19 we show the total isoscalar 2^+ response functions in the HO and THO basis. When the spin-orbit and Coulomb residual interaction are omitted, the low-lying peak belonging to the $\Omega^\pi = 0^+, 2^+$ components is shifted up in energy by about 0.2 MeV. The giant resonance is instead shifted down in energy by about 0.6 MeV with respect to the value obtained in the fully consistent calculation. The behavior of the strength functions calculated without spin-orbit and Coulomb interactions is quite close to the corresponding calculations by Yoshida *et al.* [35]. The giant resonance of our calculations is instead shifted up in energy by about 1.3 MeV respect to that in Ref. [35]. This is coherent with the former comparisons between our ISGQR and those of Yoshida *et al.* in ^{20}O where a difference of about 0.6 MeV is found, and in ^{24}Mg where there is a difference of 1.8 MeV. It seems that the blue shift displayed by the peaks in Fig. 19 as compared to those obtained in the calculations of Yoshida *et al.* without taking into account spin-orbit and Coulomb contributions in the residual interaction, increases with the intrinsic deformation of the nuclear system.

V. CONCLUSION

We described the development and testing of a fully consistent QRPA method to calculate linear response of axially-symmetric-deformed nuclei employing the canonical

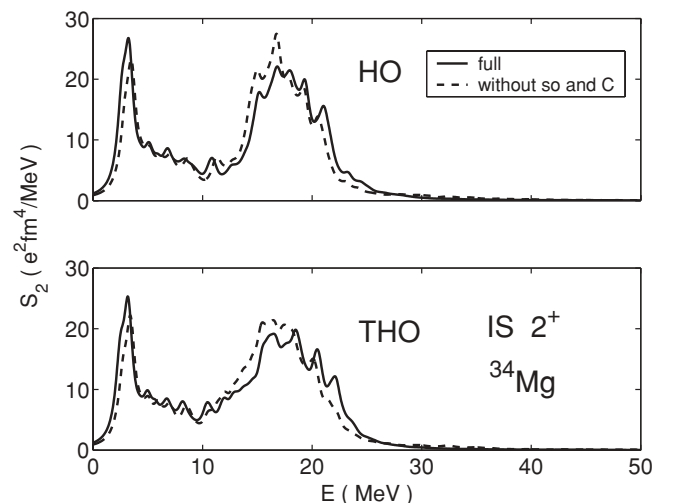


FIG. 19. The same as Fig. 10 but for ^{34}Mg .

HO or THO HFB basis. The same Skyrme force is used in both HFB and QRPA approaches in all ph, pp and hh channels. The method is applied to study the responses of ^{20}O , $^{24-26}\text{Mg}$, and ^{34}Mg .

For ^{20}O we showed the effective role of self-consistency in the IS 2^+ and IV 1^- responses. Within this context, we performed calculations with and without the spin-orbit and Coulomb terms of the residual interaction. One can conclude that for this spherical nucleus these terms mainly act on the giant resonances, shifting their centroid up in energy by several hundred keV.

We carried out detailed studies of the IS quadrupole, monopole, and IV dipole responses of deformed prolate and oblate $^{24-26}\text{Mg}$. A microscopic analysis of the low-lying IS 2^+ vibrations showed, for the open shell nucleus ^{26}Mg major contributions to the response function arising from pp transitions, while in the case of the nucleus ^{24}Mg only ph (RPA) states are found to be important. In the energy region of giant resonances, the role of deformation manifests itself in the splitting between the different projections which is more pronounced for the strongly deformed ^{24}Mg (inhomogeneous damping). On top of this splitting comes a fragmentation, especially of the highest energy projections of the giant modes. These effects lead to broad strength distributions. In this respect, our calculations confirm earlier theoretical results, and our consistent inclusion of the spin-orbit and Coulomb parts of the residual interaction only introduces minor changes concerning the giant modes, shifting the centroid by typically 1 MeV and leaving the widths rather unaffected. The calculated strength functions in regions of giant vibrations are compared to the available data, yielding generally an overall account of the experimental findings.

For ^{34}Mg , we give a description of the total IS 2^+ response concentrating on the microscopic structure of the low-lying states which are in overall accord with the theoretical results of Yoshida *et al.* [35,36].

We plan to optimize the present code, to be able to perform systematic calculations for both spherical and deformed systems in particular on the isotopes of Mg and of O. The aim is to extend our analysis to light drip line nuclei, so as to be able to study also pygmy resonances as well as other collective states typical of these exotic species. From a technical point of view, we also plan to assess for these exotic nuclear systems the significance of applying the THO basis, which should more properly take into account the extended tails of wave functions than the HO basis.

In a general perspective, the present work represents the first, unavoidable step for a consistent and more systematic study of collective modes in nuclei, in particular light exotic nuclei, taking properly into account also medium polarization effects. A study of the core polarization effects in Al isotopes has been performed by Yoshida [59] by employing the quasiparticle-vibration-coupling model on top of the deformed HFB plus QRPA using a Skyrme interaction.

The plan is to use the resulting states to calculate the role of the exchange of phonons between nucleons moving in time reversal states close to the Fermi energy has in Cooper pair binding in exotic, deformed (as well as spherical) nuclei.

ACKNOWLEDGMENTS

The authors thank J. Dobaczewski for valuable comments and discussions. They also acknowledge J. Terasaki who kindly gave the great opportunity to apply his QRPA spherical program, M. Stoitsov who provided the last version (101) of the program HFBTHO, S. Péru and K. Yoshida for the interest they have shown for this work. One of the authors (A.P.) is supported by the Academy of Finland and University of Jyväskylä within the FIDIPRO programme. C.L. acknowledges the support by a PhD stipend granted by the Science Faculty of The University of Copenhagen. The numerical calculations were performed on the supercomputers at the Consorzio Interuniversitario Lombardo Elaborazione Automatica (CILEA), Segrate, Italy.

APPENDIX: EVALUATION OF INTERACTION MATRIX ELEMENTS

A. Canonical wave functions

In this appendix we discuss the procedures used to evaluate some of the characteristic ph effective Skyrme matrix elements for the canonical wave functions having the general form:

$$\begin{aligned} \Phi_K(\mathbf{r}, \sigma) &= \frac{1}{\sqrt{2\pi}} [\varphi_{K\uparrow}(r_\perp, z) e^{i\Lambda_K \bar{\kappa} \phi} |\uparrow\rangle + \varphi_{K\downarrow}(r_\perp, z) e^{i\Lambda_K \kappa \phi} |\downarrow\rangle], \end{aligned} \quad (\text{A1})$$

with spin-up and spin-down components $\varphi_{K\uparrow}(r_\perp, z)$, $\varphi_{K\downarrow}(r_\perp, z)$ obtained in the present work in the harmonic oscillator basis, i.e., by the associated Laguerre and Hermite polynomials [60]. The general form of these matrix elements and their effective Skyrme parametrization is given by Terasaki *et al.* [14] in Eqs. (B12) to (B19). Also, for the QRPA formalism we refer to Terasaki *et al.*, Eqs. (A1)–(A6) in Ref. [14].

Concerning the most simple interactions, namely those proportional to the contact function $\delta(\mathbf{r} - \mathbf{r}')$, one has to evaluate the overlaps,

$$\begin{aligned} \langle K K' | \delta(\mathbf{r} - \mathbf{r}') | L L' \rangle &= \int d\mathbf{r} [\Phi_K^*(\mathbf{r}, \sigma) \Phi_L(\mathbf{r}, \sigma)] [\Phi_{K'}^*(\mathbf{r}, \sigma) \Phi_{L'}(\mathbf{r}, \sigma)], \end{aligned} \quad (\text{A2})$$

overlaps which in terms of the canonical wave functions (A1) read

$$\begin{aligned} \langle K K' | \delta(\mathbf{r} - \mathbf{r}') | L L' \rangle &= \frac{1}{2\pi} \delta_{\Omega_K + \Omega_{K'}, \Omega_L + \Omega_{L'}} \int r_\perp dr_\perp dz [\varphi_{K\uparrow}(r_\perp, z) \varphi_{L\uparrow}(r_\perp, z) \\ &+ \varphi_{K\downarrow}(r_\perp, z) \varphi_{L\downarrow}(r_\perp, z)] [\varphi_{K'\uparrow}(r_\perp, z) \varphi_{L'\uparrow}(r_\perp, z) \\ &+ \varphi_{K'\downarrow}(r_\perp, z) \varphi_{L'\downarrow}(r_\perp, z)]. \end{aligned} \quad (\text{A3})$$

Next, we turn to the interaction $\boldsymbol{\sigma} \cdot \boldsymbol{\sigma}' \delta(\mathbf{r} - \mathbf{r}')$. Here, the spin product is written in terms of lowering and raising spin

operators σ_+ and σ_- :

$$\boldsymbol{\sigma} \cdot \boldsymbol{\sigma}' = \frac{1}{2}[\sigma_+ \sigma'_- + \sigma_- \sigma'_+] + \sigma_z \sigma'_z. \quad (\text{A4})$$

The algebra containing the $\delta(\mathbf{r} - \mathbf{r}')$ function is the same as above, leading to the result

$$\begin{aligned} & \langle K K' | \boldsymbol{\sigma} \cdot \boldsymbol{\sigma}' \delta(\mathbf{r} - \mathbf{r}') | L L' \rangle \\ &= \frac{1}{2\pi} \delta_{\Omega_K + \Omega_{K'}, \Omega_L + \Omega_{L'}} \\ & \times \int r_\perp dr_\perp dz \{ [\varphi_{K\uparrow}(r_\perp, z) \varphi_{L\uparrow}(r_\perp, z) \\ & - \varphi_{K\downarrow}(r_\perp, z) \varphi_{L\downarrow}(r_\perp, z)] \\ & \times [\varphi_{K'\uparrow}(r_\perp, z) \varphi_{L'\uparrow}(r_\perp, z) - \varphi_{K'\downarrow}(r_\perp, z) \varphi_{L'\downarrow}(r_\perp, z)] \} \end{aligned}$$

$$\begin{aligned} & + 2[\varphi_{K\uparrow}(r_\perp, z) \varphi_{K'\downarrow}(r_\perp, z) \varphi_{L\downarrow}(r_\perp, z) \varphi_{L'\uparrow}(r_\perp, z) \\ & + \varphi_{K\downarrow}(r_\perp, z) \varphi_{K'\uparrow}(r_\perp, z) \varphi_{L\uparrow}(r_\perp, z) \varphi_{L'\downarrow}(r_\perp, z)], \end{aligned} \quad (\text{A5})$$

where one can recognize the action of $\sigma_z \sigma'_z$ in the first term, and likewise $\frac{1}{2} \sigma_+ \sigma'_-$ and $\frac{1}{2} \sigma_- \sigma'_+$ in the two subsequent terms.

It turns out that the momentum dependent parts of the residual interaction, involving differentiation in terms of the \mathbf{k} and \mathbf{k}' operators, give rise to quite many terms. Expressing one of these in full length

$$\mathbf{k}^2 = -\frac{1}{4} \nabla^2 - \frac{1}{4} \nabla'^2 + \frac{1}{2} \nabla \cdot \nabla', \quad (\text{A6})$$

one obtains

$$\begin{aligned} & \langle K K' | \delta(\mathbf{r} - \mathbf{r}') \mathbf{k}^2 | L L' \rangle \\ &= -\frac{1}{8\pi} \delta_{\Omega_K + \Omega_{K'}, \Omega_L + \Omega_{L'}} \int r_\perp dr_\perp dz \left[\varphi_{K\uparrow}(r_\perp, z) \left(\frac{1}{r_\perp} \frac{\partial}{\partial r_\perp} + \frac{\partial^2}{\partial r_\perp^2} - \frac{(\Omega_L - \frac{1}{2})^2}{r_\perp^2} + \frac{\partial^2}{\partial z^2} \right) \varphi_{L\uparrow}(r_\perp, z) \right. \\ & \left. + \varphi_{K\downarrow}(r_\perp, z) \left(\frac{1}{r_\perp} \frac{\partial}{\partial r_\perp} + \frac{\partial^2}{\partial r_\perp^2} - \frac{(\Omega_L + \frac{1}{2})^2}{r_\perp^2} + \frac{\partial^2}{\partial z^2} \right) \varphi_{L\downarrow}(r_\perp, z) \right] \\ & \times [\varphi_{K'\uparrow}(r_\perp, z) \varphi_{L'\uparrow}(r_\perp, z) + \varphi_{K'\downarrow}(r_\perp, z) \varphi_{L'\downarrow}(r_\perp, z)] \\ & - \frac{1}{8\pi} \delta_{\Omega_K + \Omega_{K'}, \Omega_L + \Omega_{L'}} \int r_\perp dr_\perp dz [\varphi_{K\uparrow}(r_\perp, z) \varphi_{L\uparrow}(r_\perp, z) + \varphi_{K\downarrow}(r_\perp, z) \varphi_{L\downarrow}(r_\perp, z)] \\ & \times \left[\varphi_{K'\uparrow}(r_\perp, z) \left(\frac{1}{r_\perp} \frac{\partial}{\partial r_\perp} + \frac{\partial^2}{\partial r_\perp^2} - \frac{(\Omega_{L'} - \frac{1}{2})^2}{r_\perp^2} + \frac{\partial^2}{\partial z^2} \right) \varphi_{L'\uparrow}(r_\perp, z) \right. \\ & \left. + \varphi_{K'\downarrow}(r_\perp, z) \left(\frac{1}{r_\perp} \frac{\partial}{\partial r_\perp} + \frac{\partial^2}{\partial r_\perp^2} - \frac{(\Omega_{L'} + \frac{1}{2})^2}{r_\perp^2} + \frac{\partial^2}{\partial z^2} \right) \varphi_{L'\downarrow}(r_\perp, z) \right] \\ & + \frac{1}{4\pi} \delta_{\Omega_K + \Omega_{K'}, \Omega_L + \Omega_{L'}} \int r_\perp dr_\perp dz \left\{ \varphi_{K\uparrow}(r_\perp, z) \varphi_{K'\uparrow}(r_\perp, z) \left[\frac{\partial \varphi_{L\uparrow}(r_\perp, z)}{\partial r_\perp} \frac{\partial \varphi_{L'\uparrow}(r_\perp, z)}{\partial r_\perp} \right. \right. \\ & \left. \left. - \frac{(\Omega_L - \frac{1}{2})(\Omega_{L'} - \frac{1}{2})}{r_\perp^2} \varphi_{L\uparrow}(r_\perp, z) \varphi_{L'\uparrow}(r_\perp, z) + \frac{\partial \varphi_{L\uparrow}(r_\perp, z)}{\partial z} \frac{\partial \varphi_{L'\uparrow}(r_\perp, z)}{\partial z} \right] \right. \\ & + \varphi_{K\uparrow}(r_\perp, z) \varphi_{K'\downarrow}(r_\perp, z) \left[\frac{\partial \varphi_{L\uparrow}(r_\perp, z)}{\partial r_\perp} \frac{\partial \varphi_{L'\downarrow}(r_\perp, z)}{\partial r_\perp} - \frac{(\Omega_L - \frac{1}{2})(\Omega_{L'} + \frac{1}{2})}{r_\perp^2} \varphi_{L\uparrow}(r_\perp, z) \varphi_{L'\downarrow}(r_\perp, z) \right. \\ & \left. + \frac{\partial \varphi_{L\uparrow}(r_\perp, z)}{\partial z} \frac{\partial \varphi_{L'\downarrow}(r_\perp, z)}{\partial z} \right] + \varphi_{K\downarrow}(r_\perp, z) \varphi_{K'\uparrow}(r_\perp, z) \left[\frac{\partial \varphi_{L\downarrow}(r_\perp, z)}{\partial r_\perp} \frac{\partial \varphi_{L'\uparrow}(r_\perp, z)}{\partial r_\perp} \right. \\ & \left. - \frac{(\Omega_L + \frac{1}{2})(\Omega_{L'} - \frac{1}{2})}{r_\perp^2} \varphi_{L\downarrow}(r_\perp, z) \varphi_{L'\uparrow}(r_\perp, z) + \frac{\partial \varphi_{L\downarrow}(r_\perp, z)}{\partial z} \frac{\partial \varphi_{L'\uparrow}(r_\perp, z)}{\partial z} \right] \\ & \left. + \varphi_{K\downarrow}(r_\perp, z) \varphi_{K'\downarrow}(r_\perp, z) \left[\frac{\partial \varphi_{L\downarrow}(r_\perp, z)}{\partial r_\perp} \frac{\partial \varphi_{L'\downarrow}(r_\perp, z)}{\partial r_\perp} - \frac{(\Omega_L + \frac{1}{2})(\Omega_{L'} + \frac{1}{2})}{r_\perp^2} \varphi_{L\downarrow}(r_\perp, z) \varphi_{L'\downarrow}(r_\perp, z) \right. \right. \\ & \left. \left. + \frac{\partial \varphi_{L\downarrow}(r_\perp, z)}{\partial z} \frac{\partial \varphi_{L'\downarrow}(r_\perp, z)}{\partial z} \right] \right\}. \end{aligned} \quad (\text{A7})$$

B. Spin-orbit interaction

The spin-orbit term $i(\boldsymbol{\sigma} + \boldsymbol{\sigma}') \cdot \mathbf{k}^\dagger \times \delta(\mathbf{r} - \mathbf{r}')\mathbf{k}$ of the residual interaction is likely the most involved to evaluate. However, it becomes conceptually simple when it is interpreted as a volume product of three vectors $\mathbf{A} \cdot (\mathbf{B} \times \mathbf{C})$. Next, the cartesian components of the vectors are replaced by the components of the spherical tensors of rank 1 [61]. This bears some resemblance to the treatment in the spherical case [14]. In the deformed case, the spin spherical tensors raising and lowering operators, and the spherical tensors of the differential operators also acquire a more simple form than their Cartesian counterparts, as they can be expressed in terms of raising and lowering operators as

$$\nabla_+ = e^{i\phi} \left(\frac{\partial}{\partial r_\perp} + \frac{i}{r_\perp} \frac{\partial}{\partial \phi} \right), \quad (\text{A8})$$

and

$$\nabla_- = e^{-i\phi} \left(\frac{\partial}{\partial r_\perp} - \frac{i}{r_\perp} \frac{\partial}{\partial \phi} \right). \quad (\text{A9})$$

Still, the volume product contains six terms, namely,

$$\begin{aligned} & \langle KK' | i(\boldsymbol{\sigma} + \boldsymbol{\sigma}') \cdot \mathbf{k}^\dagger \times \delta(\mathbf{r} - \mathbf{r}')\mathbf{k} | LL' \rangle \\ &= \frac{1}{8} [\langle KK' | (\sigma_+ + \sigma'_+) (\nabla_z - \nabla'_z) \delta(\mathbf{r} - \mathbf{r}') (\nabla_- - \nabla'_-) | LL' \rangle \\ & - \langle KK' | (\sigma_+ + \sigma'_+) (\nabla_- - \nabla'_-) \delta(\mathbf{r} - \mathbf{r}') (\nabla_z - \nabla'_z) | LL' \rangle \\ & + \langle KK' | (\sigma_z + \sigma'_z) (\nabla_- - \nabla'_-) \delta(\mathbf{r} - \mathbf{r}') (\nabla_+ - \nabla'_+) | LL' \rangle \\ & - \langle KK' | (\sigma_z + \sigma'_z) (\nabla_+ - \nabla'_+) \delta(\mathbf{r} - \mathbf{r}') (\nabla_- - \nabla'_-) | LL' \rangle \\ & + \langle KK' | (\sigma_- + \sigma'_-) (\nabla_+ - \nabla'_+) \delta(\mathbf{r} - \mathbf{r}') (\nabla_z - \nabla'_z) | LL' \rangle \\ & - \langle KK' | (\sigma_- + \sigma'_-) (\nabla_z - \nabla'_z) \delta(\mathbf{r} - \mathbf{r}') (\nabla_+ - \nabla'_+) | LL' \rangle] \end{aligned} \quad (\text{A10})$$

In the above relation, the operators to the left of $\delta(\mathbf{r} - \mathbf{r}')$ act on K, K' , while the operators to the right of $\delta(\mathbf{r} - \mathbf{r}')$ act on L, L' . The sum over the six terms of Eq. (A10) corresponds to a sum over the six permutations of the set $\{+, z, -\}$.

C. Coulomb interaction

Due to the short-range character of the nuclear residual interaction, which is expressed through the $\delta(\mathbf{r} - \mathbf{r}')$ functions, the four-dimensional integrals $\int r_\perp dr_\perp dz r'_\perp dr'_\perp dz'$ are directly replaced by two-dimensional integrals. However, for the direct term of the Coulomb interaction $V_{direct}^{eff} = \frac{e^2}{|\mathbf{r} - \mathbf{r}'|}$ one needs to carry out the full integration. In order to exploit the cylindrical symmetry, we make use of an expansion method

applied to astrophysical problems by Cohl and Tohline [62,63]

$$\frac{1}{|\mathbf{r} - \mathbf{r}'|} = \frac{1}{\pi \sqrt{r_\perp r'_\perp}} \sum_{m=-\infty}^{\infty} Q_{m-\frac{1}{2}}(\chi_-) e^{im(\phi - \phi')}, \quad (\text{A11})$$

where

$$\chi_- \equiv \frac{r_\perp^2 + r'^2_\perp + (z - z')^2}{2r_\perp r'_\perp}, \quad (\text{A12})$$

Here $Q_{m-\frac{1}{2}}$ is a Legendre function of the second kind of half-integer degree [60]. We have checked the convergence of this expansion, which is quite rapid when the parameter χ is not too close to 1. Inserting the canonical wave functions, the integrals over the azimuthal angle select the order m of the projection of the angular momentum on the z axis, such that $m = \Omega_K - \Omega_L = \Omega_{L'} - \Omega_{K'}$. The functions $Q_{m-\frac{1}{2}}$ can readily be evaluated by simple integrals and tabulated over a suitable range. In the calculation of the matrix element

$$\begin{aligned} \langle KK' | V_{direct}^{eff} | LL' \rangle &= \iint d\mathbf{r} d\mathbf{r}' \times \Phi_K^*(\mathbf{r}, \boldsymbol{\sigma}) \Phi_{K'}^*(\mathbf{r}', \boldsymbol{\sigma}) \\ &\times \frac{e^2}{|\mathbf{r} - \mathbf{r}'|} \Phi_L(\mathbf{r}, \boldsymbol{\sigma}) \Phi_{L'}(\mathbf{r}', \boldsymbol{\sigma}), \end{aligned} \quad (\text{A13})$$

it is important to take into account the symmetry of the wave functions

$$\Phi_K(-\mathbf{r}, \boldsymbol{\sigma}) = \pi_K \Phi_K(\mathbf{r}, \boldsymbol{\sigma}), \quad (\text{A14})$$

$\pi_K = \pm 1$ being the parity of the state K depending on the sign of z . By exploiting these symmetries one needs only to carry out integration over $z, z' > 0$, aside from integration over the two angles ϕ and ϕ'

$$\begin{aligned} & \langle KK' | V_{direct}^{eff} | LL' \rangle \\ &= 2e^2 (2\pi)^2 \delta_{m, \Omega_K - \Omega_L} \cdot \delta_{m, \Omega_{L'} - \Omega_{K'}} \\ &\times \int_0^\infty r_\perp dr_\perp \int_0^\infty r'_\perp dr'_\perp \int_0^\infty dz \int_0^\infty dz' \\ &\times [\varphi_{K\uparrow}(r_\perp, z) \varphi_{L\uparrow}(r_\perp, z) + \varphi_{K\downarrow}(r_\perp, z) \varphi_{L\downarrow}(r_\perp, z)] \\ &\times \frac{Q_{m-\frac{1}{2}}(\chi_-) + \pi_{K'} \cdot \pi_{L'} \cdot (-1)^m Q_{m-\frac{1}{2}}(\chi_+)}{\pi \sqrt{r_\perp r'_\perp}} \\ &\times [\varphi_{K'\uparrow}(r'_\perp, z') \varphi_{L'\uparrow}(r'_\perp, z') + \varphi_{K'\downarrow}(r'_\perp, z') \varphi_{L'\downarrow}(r'_\perp, z')], \end{aligned} \quad (\text{A15})$$

with

$$\chi_+ = \frac{r_\perp^2 + r'^2_\perp + (z + z')^2}{2r_\perp r'_\perp}. \quad (\text{A16})$$

Since $\pi_{K'} \cdot \pi_{L'} \cdot (-1)^m$ does not depend on the projections $\Omega_K - \Omega_L, \Omega_{L'} - \Omega_{K'}$, this factor is the same for spin-up and spin-down wave functions.

- [1] A. Bohr and B. R. Mottelson, *Nuclear Structure*, Vol. II (Benjamin, Reading, MA, 1969, 1975).
 [2] S. Dattagupta, *Relaxation Phenomena in Condensed Matter Physics* (Academic Press, Orlando, 1987).

- [3] P. F. Bortignon, A. Bracco, and R. A. Broglia, *Giant Resonances, Nuclear Structure at Finite Temperature* (Harwood Academic Press, Amsterdam, 1998).
 [4] P. Carlos *et al.*, *Nucl. Phys. A* **172**, 437 (1971).

- [5] D. Sackett *et al.*, *Phys. Rev. C* **48**, 118 (1993).
- [6] F. Barranco *et al.*, *Eur. Phys. J. A* **11**, 385 (2001).
- [7] I. Hamamoto, H. Sagawa, and X. Z. Zhang, *Phys. Rev. C* **53**, 765 (1996).
- [8] S. Shlomo and B. K. Agrawal, *Nucl. Phys. A* **722**, 98c (2003).
- [9] M. Matsuo, *Nucl. Phys. A* **696**, 371 (2001).
- [10] K. Hagino and H. Sagawa, *Nucl. Phys. A* **695**, 82 (2001).
- [11] M. Bender, J. Dobaczewski, J. Engel, and W. Nazarewicz, *Phys. Rev. C* **65**, 054322 (2002).
- [12] E. Khan, N. Sandulescu, M. Grasso, and N. V. Giai, *Phys. Rev. C* **66**, 024309 (2002).
- [13] M. Yamagami and N. Van Giai, *Phys. Rev. C* **69**, 034301 (2004).
- [14] J. Terasaki, J. Engel, M. Bender, J. Dobaczewski, W. Nazarewicz, and M. Stoitsov, *Phys. Rev. C* **71**, 034310 (2005).
- [15] D. Vretenar, N. Paar, P. Ring, and G. A. Lalazissis, *Nucl. Phys. A* **692**, 496 (2001).
- [16] N. Paar, P. Ring, T. Niksić, and D. Vretenar, *Phys. Rev. C* **67**, 034312 (2003).
- [17] N. Paar, T. Niksić, D. Vretenar, and P. Ring, *Phys. Rev. C* **69**, 054303 (2004).
- [18] N. Paar, T. Niksić, T. D. Vretenar, and P. Ring, *Phys. Lett. B* **606**, 288 (2005).
- [19] L. G. Cao and Z. Y. Ma, *Phys. Rev. C* **71**, 034305 (2005).
- [20] D. Vretenar, A. V. Afanasjev, G. A. Lalazissis, and P. Ring, *Phys. Rep.* **409**, 101 (2005).
- [21] G. Giambrone, S. Scheit, F. Barranco, P. F. Bortignon, G. Colò, D. Sarchi, and E. Vigezzi, *Nucl. Phys. A* **726**, 3 (2003).
- [22] D. Sarchi, P. F. Bortignon, and G. Colò, *Phys. Lett. B* **601**, 27 (2004).
- [23] J. Toivanen, B. G. Carlsson, J. Dobaczewski, K. Mizuyama, R. R. Rodríguez-Guzmán, P. Toivanen, and P. Veselý, *Phys. Rev. C* **81**, 034312 (2010).
- [24] T. Nakatsukasa, T. Inakura, and K. Yabana, *Phys. Rev. C* **76**, 024318 (2007).
- [25] T. Inakura, T. Nakatsukasa, and K. Yabana, *Phys. Rev. C* **80**, 044301 (2009).
- [26] T. Nakatsukasa and K. Yabana, *Phys. Rev. C* **71**, 024301 (2005).
- [27] T. Inakura, H. Imagawa, Y. Hashimoto, S. Mizutori, M. Yamagami, and K. Matsuyanagi, *Nucl. Phys. A* **768**, 61 (2006).
- [28] P. Urkedal, X. Z. Zhang, and I. Hamamoto, *Phys. Rev. C* **64**, 054304 (2001).
- [29] R. Álvarez-Rodríguez, P. Sarriguren, E. Moya de Guerra, L. Paceaescu, A. Faessler, and F. Simkovic, *Phys. Rev. C* **70**, 064309 (2004).
- [30] J. Dobaczewski, H. Flocard, and J. Treiner, *Nucl. Phys. A* **422**, 103 (1984).
- [31] K. Bennaceur and J. Dobaczewski, *Comput. Phys. Commun.* **168**, 96 (2005).
- [32] J. Dobaczewski, W. Nazarewicz, T. R. Werner, J. F. Berger, C. R. Chinn, and J. Dechargé, *Phys. Rev. C* **53**, 2809 (1996).
- [33] M. Stoitsov, J. Dobaczewski, W. Nazarewicz, and P. Ring, *Comput. Phys. Commun.* **167**, 43 (2005).
- [34] S. Péru and H. Goutte, *Phys. Rev. C* **77**, 044313 (2008).
- [35] K. Yoshida and N. V. Giai, *Phys. Rev. C* **78**, 064316 (2008).
- [36] K. Yoshida and M. Yamagami, *Phys. Rev. C* **77**, 044312 (2008).
- [37] R. R. Chasman, *Phys. Rev. C* **14**, 1935 (1976).
- [38] J. Bartel, P. Quentin, M. Brack, C. Guet, and H.-B. Håkasson, *Nucl. Phys. A* **386**, 79 (1982).
- [39] N. J. Stone, *At. Data Nucl. Data Tables* **90**, 75 (2005).
- [40] M. Carchidi, B. H. Wildenthal, and B. A. Brown, *Phys. Rev. C* **34**, 2280 (1986).
- [41] P. Ring and P. Schuck, *The Nuclear Many-Body Problem* (Springer Verlag, New York, 1980).
- [42] J. Terasaki and J. Engel, *Phys. Rev. C* **74**, 044301 (2006).
- [43] D. J. Thouless, *Nucl. Phys.* **22**, 78 (1961).
- [44] S. Péru, J. F. Berger, and P. F. Bortignon, *Eur. Phys. J. A* **26**, 25 (2005).
- [45] P. M. Endt, *Nucl. Phys. A* **521**, 1 (1990).
- [46] J. D. Garrett, H. T. Fortune, R. Middleton, and W. Scholz, *Phys. Rev. C* **18**, 2032 (1978).
- [47] H. Zarek *et al.*, *Phys. Lett. B* **80**, 26 (1978).
- [48] K. Van Der Borg, M. N. Harakeh, and B. S. Nilsson, *Nucl. Phys. A* **325**, 31 (1979).
- [49] G. S. Blanpied *et al.*, *Phys. Rev. C* **41**, 1625 (1990).
- [50] F. Barranco, R. A. Broglia, G. Gori, E. Vigezzi, P. F. Bortignon, and J. Terasaki, *Phys. Rev. Lett.* **83**, 2147 (1999).
- [51] P. Donati *et al.*, *J. Phys. G* **31**, 295 (2005).
- [52] D. H. Youngblood, Y.-W. Lui, and H. L. Clark, *Phys. Rev. C* **60**, 014304 (1999).
- [53] K. M. Irgashev, B. S. Ishkhanov, and I. M. Kapitonov, *Phys. Rev.* **145**, 771 (1966).
- [54] O. Titze, E. Spamer, and A. Goldmann, *Phys. Lett. B* **24**, 169 (1967).
- [55] O. Titze, A. Goldmann, and E. Spamer, *Phys. Lett. B* **31**, 565 (1970).
- [56] S. C. Fultz, R. A. Alvarez, B. L. Berman, M. A. Kelly, D. R. Lasher, T. W. Phillips, and J. McElhinney, *Phys. Rev. C* **4**, 149 (1971).
- [57] B. S. Ishkhanov, I. M. Kapitonov, E. V. Lazutin, I. M. Piskarev, and V. G. Shevchenko, *Nucl. Phys. A* **186**, 438 (1972).
- [58] J. Dobaczewski, W. Nazarewicz, T. R. Werner, J. F. Berger, C. R. Chinn, and J. Decharge, *Phys. Rev. C* **53**, 2809 (1996).
- [59] K. Yoshida, *Phys. Rev. C* **79**, 054303 (2009).
- [60] M. Abramowitz and I. A. Stegun, *Handbook of Mathematical Functions* (Dover, New York, 1970).
- [61] A. Bohr and B. R. Mottelson, *Nuclear Structure*, Vol. I (Benjamin, Reading, MA, 1969, 1975).
- [62] H. S. Cohl and J. E. Tohline, *Astr. Journ.* **527**, 86 (1999).
- [63] H. S. Cohl, A. R. P. Rau, J. E. Tohline, D. A. Browne, J. E. Cazes, and E. I. Barnes, *Phys. Rev. A* **64**, 052509 (2001).